Dynamics of reentry around a circular obstacle in cardiac tissue

Fagen Xie, Zhilin Qu, and Alan Garfinkel
Department of Medicine (Cardiology) and Department of Physiological Science, University of California at Los Angeles, Los Angeles, California 90095

(Received 11 February 1998; revised manuscript received 24 June 1998)

We studied the dynamics of a wave propagating around a circular obstacle in a two-dimensional cardiac tissue model. By starting with a large obstacle and decreasing its radius, a continuous transition was created between the two major types of reentrant cardiac arrhythmias: anatomical reentry (essentially one-dimensional) and functional reentry. As the radius of the obstacle decreases, a sequence of transitions occurs, from periodic motion to a modulated period-2 rhythm, and then to spiral wave breakup. These results may provide a useful basis for refining cardiac ablation techniques currently in use. [S1063-651X(98)06311-9]

PACS number(s): 87.10.+e, 05.45.+b, 87.22.As

Reentrant excitation, in which a wave of excitation ''reenters'' territory it has previously excited, is the leading mechanism of cardiac tachyarrhythmias. The first experimental model of reentry was generated by Mines [1] in a ring of cardiac muscle derived from a dog heart. (A similar preparation was studied by Frame and Simson [2].) Complex structures in the heart, especially in the atria and atrioventricular node, provide excellent substrates for this type of reentry, which can be modeled as a one-dimensional circular pathway. One-dimensional reentry is also a useful model for reentry around circular obstacles, like those formed by infarct scars. But not all reentry can be simplified to the one-dimensional model: the experiments of Allessie's group [3] have demonstrated that reentry can occur without an obstacle or other anatomically defined path. This kind of reentry has been shown experimentally to consist of spiral or scroll waves [4,5] in accord with nonlinear theory [6–8], and requires at least a two-dimensional excitable medium to simulate. The 1D case is now referred to as ''anatomical reentry'' and the higher-dimensional (2D or 3D) as ''functional reentry.'' The case of reentry around an obstacle is a kind of intermediate case.

Experiments on reentry around an obstacle in cardiac tissue [1,2,9] showed that reducing the obstacle size or prolonging the wavelength promoted complex oscillations, conduction failure, and complex spiral wave behaviors. Experiments studying chemical waves in CO oxidation in an annular domain showed that complex behaviors occur in larger rings [10], they also found that the frequency of a spiral wave in a circular domain depends on domain size [10]. Simulations in excitable media with circular domains [11,12] and in rings of cardiac cells [13] showed that the rotating frequency and pulse behaviors were size dependent. In this paper, we study cardiac propagation in a 2D circular domain with a circular obstacle (a hole with no-flux boundary) in the center. By shrinking the radius of the hole, we can continuously change the system from a 1D ring to 2D tissue with an obstacle, and finally to homogeneous 2D tissue. With this protocol, we can study the relation between the two types of reentry, and between 1D dynamics and 2D dynamics.

Ignoring the microscopic cell structure, electrical impulse conduction in cardiac tissue can be described by the partial differential equation

$$\partial V/\partial t = -I_{\rm ion}/C_m + D\nabla^2 V, \tag{1}$$

where V is the membrane voltage (mV), $C_m = 1\ \mu\mathrm{F\,cm^{-2}}$ is the membrane capacitance, and $D = 1\ \mathrm{cm^2/s}$ is the diffusion coefficient. $I_{\rm ion} = I_{\rm Na} + I_{\rm si} + I_{\rm K} + I_{K1} + I_{Kp} + I_b$ is the total cellular transmembrane ionic current density from the Luo-Rudy ventricular action potential model [14]. $I_{\rm Na} = \bar{G}_{\rm Na} m^3 h j (V - 54.4)$ is the fast inward Na^+ current; $I_{\rm si} = \bar{G}_{\rm si} d f (V - E_{\rm si})$ is the slow inward Ca^{2+} current; $I_{\rm K} = \bar{G}_{\rm K} x x (V - 77)$ is the time-dependent outward K^+ current; $I_{\rm K1}$, $I_{\rm Kp}$, and I_b, which are solely functions of V, are the time-independent outward K^+ current, plateau K^+ current, and background current, respectively. m, h, j, d, f, and x are gating variables, all governed by the same type of ordinary differential equation. For details of the equations and functions see Ref. [14]. In our simulations we set $\bar{G}_{\rm Na} = 23\ \mathrm{mS}/\mu\mathrm{F}$, $\bar{G}_{\rm K} = 0.705\ \mathrm{mS}/\mu\mathrm{F}$, $\bar{G}_{\rm si} = 0.07\ \mathrm{mS}/\mu\mathrm{F}$. To solve Eq. (1) in a 2D circular domain, we integrated it in a polar coordinate system with no-flux boundary conditions at both boundaries: $\partial V/\partial r|_{r=R} = \partial V/\partial r|_{r=r_0} = 0$, where R is the domain radius and r_0 the obstacle radius. When $r_0 = 0$, the system becomes 2D homogeneous tissue, and when $r_0 = R$, it collapses into a one-dimensional ring. Because of the stiffness of the upstroke of the action potential, a very small time step must be used to integrate Eq. (1). To overcome this disadvantage, we split the reaction operator and the diffusion operator in Eq. (1) using the well-known operator-splitting method [16]. We then integrated the reaction term using a second-order Runge-Kutta method with an adaptive time step that depends on the derivative of voltage, and the diffusion term with an alternating-direction implicit method to guarantee numerical stability. In this study, the adaptive time step varied from $\Delta t_{\rm min} = 0.01$ ms to $\Delta t_{\rm max} = 0.2$ ms. The diffusion term was integrated with the maximum time step $\Delta t = \Delta t_{\rm max} = 0.2$ ms to keep all cells synchronized. Numerical simulation [15] showed that when $\Delta t_{\rm max} = 0.01$ ms to $\Delta t_{\rm max} = 0.2$ ms, the relative error was less than 2%. The space steps are $\Delta\theta = 2\pi/1000$, and $\Delta r = 0.02$ cm. Because we use an implicit method, numerical stability is maintained even for very small r_0. When $r_0 = 0$, the center point becomes a singularity in the polar discretization system, and

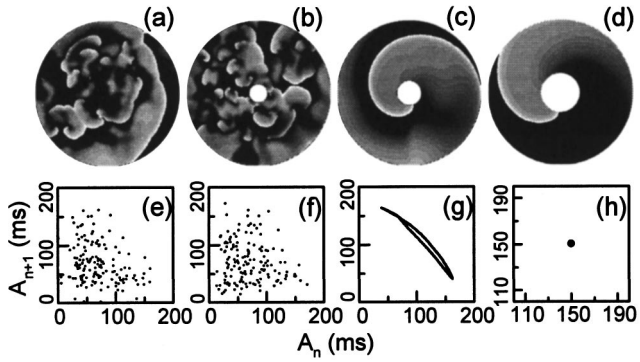

FIG. 1. A sequence of transitions, from fibrillationlike activity to a periodic anchored spiral wave, as the obstacle radius r_0 increases, for a fixed $R=9.2$-cm outer radius. (a)–(d) Voltage snapshots (voltage values decreasing from white to black) in the tissue for (a) $r_0=0.0$ cm; (b) $r_0=1.20$ cm; (c) $r_0=1.60$ cm; (d) $r_0=2.50$ cm. Note the transition from a multispiral state to a single anchored spiral. (e)–(h) Action potential duration (A) return maps corresponding to (a)–(d), respectively. Note the transition from high-dimensional to quasiperiodic to periodic behavior.

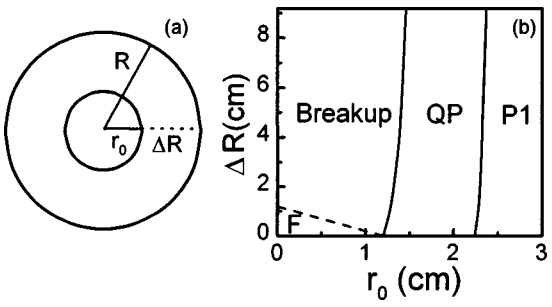

FIG. 2. (a) Schematic of the cardiac tissue. (b) Phase diagram in the r_0–ΔR plane. $P1$, period-1 anchored wave; QP, quasiperiodic anchored wave; Breakup, spiral wave breakup; F, failure of wave propagation.

we use in its place the average value of its 1000 immediately surrounding neighbors. This gives the correct action potential of the center point. Since we are studying the stability of reentry around an obstacle, we always initiate the spiral wave near the obstacle by two perpendicular waves. If the spiral waves are initiated far away from the obstacle boundary, more complex behaviors can exist.

The dynamical properties of this system depend heavily on R and r_0. Fig. 1 shows a set of simulation results for different r_0 but fixed $R(=9.2$ cm). Without an obstacle ($r_0=0$), a spiral wave initiated by two successive perpendicular waves breaks up into fibrillatory like motion after several rotations, as has been shown to occur in normal cardiac tissue [5]. A snapshot of the disordered spatial distribution of voltage in this state is shown in Fig. 1(a). The corresponding Poincaré return map for the action potential duration (A) [17], shown in Fig. 1(e), indicates that the system is in high-dimensional chaos. Now we place an obstacle in the tissue, i.e., we increase r_0 from zero. If the obstacle is small, the behavior of the system is like that for $r_0=0$: an initiated spiral wave breaks up into fibrillatory like motion after several rotations. Figures. 1(b) and 1(f) show a voltage snapshot and action potential duration return map. Note that they resemble the case without an obstacle. But as r_0 is increased beyond a critical value ($r_{0c1}\approx 1.44$ cm), the behavior of the system abruptly changes. An initiated spiral wave does not break up; instead it attaches (''anchors'') to the obstacle. In fact, the curved, propagating wave is no longer a true spiral wave, since it lacks a tip. The dynamics is no longer chaotic but quasiperiodic. A quasiperiodic wave anchored to an obstacle is shown in Fig. 1(c) and its action potential duration return map is shown in Fig. 1(g). As the radius of the obstacle is increased beyond another critical value ($r_{0c2}\approx 2.35$ cm), another transition occurs, as the quasiperiodicity is abruptly replaced by a period-1 motion. Figures 1(d) and (h) show a periodic anchored wave and its action potential duration return map.

We then explored parameter space by varying both R and r_0. Figure 2 shows the phase diagram of the system in the r_0-ΔR parameter plane ($\Delta R=R-r_0$). It consists of four regions: stable period-1 ($P1$) conduction, quasiperiodic (QP) alternans (a period-2 rhythm amplitude modulated at a longer period), spiral wave breakup (Breakup), and complete conduction failure (F). The critical line between spiral wave breakup and conduction failure is $r_0+\Delta R=r_{0c1}\approx 1.20$ cm, which is the critical point (corresponding to ring length ~ 7.5 cm) for conduction failure in the 1D ring.

A surprising and interesting result is that the critical curves distinguishing breakup from QP, and QP from P1, are nearly vertical except near values of $R\approx r_0$. This means that no matter how large the tissue size R is, the dynamics of the system is almost entirely determined by r_0, except for the boundary between the failure and breakup regions. *This is because r_0 largely determines cycle length (the period of the wave, T) for sufficiently large r_0, and T largely determines the dynamics.*

To better understand the results shown in Fig. 2, let us first summarize the known results from ring simulations, which corresponds to $R=r_0$ in our case. Studies [13] have shown that the dynamics in the ring depends on both action potential duration and conduction velocity (C) restitution properties, and on the ring length $L(=2\pi R=2\pi r_0)$. If the slope of the action potential duration restitution curve (at the equilibrium state) is less than **1**, the system is stable, and propagation will be periodic if the ring is long enough, or else it will fail. But if the slope of the action potential duration restitution curve is greater than **1** at the equilibrium state, propagation can be persistent yet unstable. For a range of values of L, the system will display quasiperiodic motion, modulated alternans (period-2 rhythm), while if L is too short, conduction failure occurs. In a ring, L selects the basic rotation frequency; the steepness of the action potential duration restitution causes the cycle-length-dependent instability and thus the alternans, and conduction velocity restitution selects the modulation frequency (quasiperiodicity) [13]. In our simulations, the ring corresponds to small values of ΔR; a path traversed at low ΔR from large r_0 to small, corresponding to going from large L to small in a ring, reproduces the behavior previously seen in the ring: from period-1 to modulated (quasiperiodic) alternans, and then to conduction failure.

The 2D simulation diverges from the ring model as ΔR becomes significantly nonzero. To study the 2D case, we will

start with $R=r_0$ sufficiently large that the propagation is periodic, and then progressively reduce r_0 to make the system truly 2D.

The first phenomenon that is encountered as r_0 shrinks away from R is the appearance of wave-front curvature. As a consequence of the no-flux boundary condition, the wave front must be perpendicular to both boundaries. But a completely rectilinear wave front cannot exist here, because $T=2\pi r_0/C_{r_0}=2\pi R/C_R$ must be satisfied to have a unique T in the system. Only a curved wave front can meet this requirement. According to the eikonal relation $C=C_0-D\kappa$, positive curvature must form at r_0 and negative curvature must form at R to fulfill the cycle length requirement. Due to the curvature effect, the system will select a T that is longer than that of a ring with $L=2\pi r_0$ but shorter than that of a ring with $L=2\pi R$.

If r_0 is further shortened to r_{0c2} to select a T for which the slope of action potential duration restitution is greater than **1**, then the propagating wave will begin to oscillate in modulated alternans. If ΔR is large enough, this oscillation will be desynchronized in space and will make the wave back scalloped [Fig. 1(c)]. Finally, if r_0 is further shortened to r_{0c1}, selecting a T for which conduction failure occurs due to wave back scalloping, then spiral breakup takes place at those failure points. This creates spatiotemporally chaotic motion.

Although the T, and thus the stability of the circulating wave, is mostly determined by the radius r_0 of the obstacle, the boundary lines in Fig. 2 are not completely vertical, indicating a small effect of ΔR. This can be understood as due to the effects of curvature. As ΔR grows from 0, the presence of curvature in the wave front implies, by the eikonal relation, that the wave speed will be lower than that in the $\Delta R=0$ case. Lowered wave speed by itself would imply that the wave was made more stable by the presence of ΔR, which is the opposite of what is seen in Fig. 2. The line separating periodic and quasiperiodic, and the line separating quasiperiodic and breakup, shifts to the right as ΔR gets larger, indicating that for larger ΔR, the wave is less stable, because instability comes at higher values of r_0. The explanation for this effect is that, as discussed above, the no-flux boundary condition requires the wave to be perpendicular to the boundaries, which in turn requires the wave to have negative curvature at the outer boundary R. Although the positive curvature near the obstacle has a stabilizing effect on the action potential duration restitution curve [18], the negative curvature at the outer boundary has the opposite effect. Figure 3 shows plots of A_n versus I_n (I_n is defined as T_n-A_n) near the obstacle [(a), open circles] and near the boundary [(b), closed circles] just after the onset of quasiperiodicity. Note that the oscillation near the outer boundary is larger than that near the obstacle. This causes the spiral wave instability to first develop at the outer boundary, then propagate inward.

To give a quantitative view of these results, Fig. 4 shows the maximum and minimum values of A, and the average cycle length ($\langle T\rangle$), versus r_0, from simulations of the ring and 2D tissue. First, note the first bifurcation that occurs as r_0 decreases. This is the bifurcation to quasiperiodic alternans. This bifurcation was observed by several authors [13].

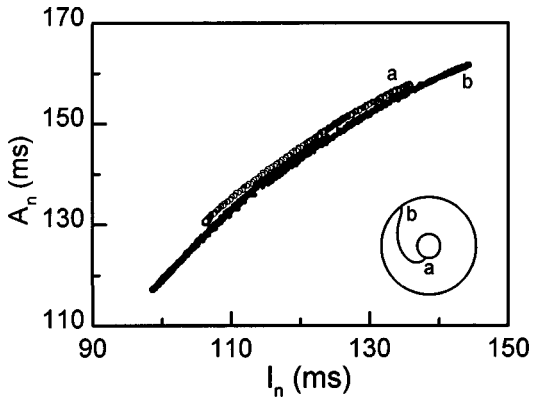

FIG. 3. A_n vs I_n plots near the obstacle [(a), open circles] and the outside boundary [(b), closed circles] for $R=9.2$ cm, $r_0=2.32$ cm. A schematic wave front is shown at the lower right (curvature is exaggerated).

Note also that for decreasing r_0, the bifurcations in 2D occur sooner than they do in the ring, which is the result expected from our argument above. Second, the oscillation amplitude is slightly larger, and $\langle T\rangle$ is slightly longer, in 2D than in the ring. The increase in maximum A and decrease of minimum A are due to the instability from R, but the increasing of $\langle T\rangle$ is due to the slowing down of the wave front at r_0. Third, sudden transitions occur in both A and $\langle T\rangle$ at the second bifurcation point in 2D, i.e., the transition from QP to breakup; $\langle T\rangle$ remains unchanged as r_0 decreases beyond the transition point. These results differ from previous studies [11,12] in which reentry is always stable for decreasing r_0, and in which the cycle length versus r_0 is continuous, and decreases continuously with decreasing r_0 until a minimum value is reached. The discontinuity in our simulation occurs because spiral breakup occurs, and once spiral breakup takes place somewhere in the tissue, the cycle length of the newly formed spiral wave will be selected by its own dynamics rather than by the obstacle. Thus, when the system develops into fully developed spatiotemporal chaos, a number of wavelets meander through the tissue, and no wave anchors to the obstacle. In this case, the obstacle has lost its influence on the wave rotation frequency. The average cycle length therefore changes abruptly, and is thereafter unaffected by the presence or absence of small obstacles.

In conclusion, we explored the dynamical relation of propagation in a 1D ring and in 2D tissue with an obstacle.

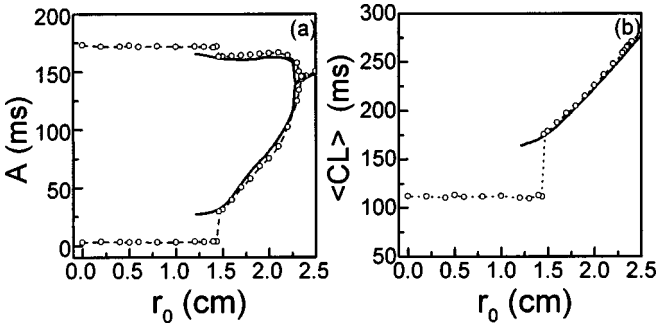

FIG. 4. Bifurcations produced by changing r_0 both in the ring (solid lines) and in 2D tissue (open circles) (outer $R=9.2$ cm). (a) The minimum and maximum A vs r_0. (b) Average T vs r_0.

We saw a transition from periodic to quasiperiodic motion via Hopf bifurcation, as was seen in the ring, and a transition to spiral wave breakup and spatiotemporal chaos in 2D tissue corresponding to conduction failure in the ring. The mechanism of spiral wave breakup and the transition to spatiotemporal chaos in homogeneous tissue was also studied in Refs. [7,18], but the strategy there was to alter action potential duration restitution. Here, by keeping the same action potenital duration restitution, but changing the obstacle radius (and thus the cycle length), we again found spiral wave breakup and a transition to spatiotemporal chaos. The two strategies can be unified by the observation that for a given action potential duration restitution curve, the cycle length determines where on the curve the system will fall, and hence its stability. For a sufficiently large cycle length, forced by a sufficiently large obstacle, the system will be pushed to the flat part of the restitution curve, resulting in stable conduction.

This study gives a mechanism for spiral wave anchoring, a phenomenon well known in real cardiac tissue [9]. Anchoring, we suggest, is due to the stabilizing effect of increased cycle length due to a sufficiently large obstacle. Our simulations have the surprising consequence that *a sufficiently large obstacle in a tissue tends to make reentry more stable*, in contrast to the conventional cardiologic wisdom that obstacles tend to cause breakup. We find that an anatomically reentrant wave is more stable than the corresponding functionally reentrant wave in the same tissue.

Our study has implications for the clinical procedures currently used to prevent fibrillation. One of the standard clinical procedures for patients with atrial fibrillation is catheter ablation, in which lines or arcs of nonconducting lesions are created to confine cardiac wave propagation. Our study defines a rational basis for this procedure, and provides a criterion for how large the lesions must be to prevent the spiral breakup that drives fibrillation.

This work was supported by NIH Grant No. P50 HL52319, and by the American Heart Association, Greater Los Angeles Affiliate (F.X. & Z.Q.). We thank Dr. James N. Weiss for helpful conversations.

[1] G. Mines, Trans. R. Soc. Can. **4**, 43 (1914).
[2] L. Frame and M. Simson, Circ. Res. **78**, 1277 (1988).
[3] M. Allessie *et al.*, Circ. Res. **33**, 54 (1973); **39**, 168 (1976); **41**, 9 (1977).
[4] J. Davidenko *et al.*, Nature (London) **355**, 349 (1992); A. Pertsov *et al.*, Circ. Res. **72**, 631 (1993); R. Gray *et al.*, Science **270**, 1222 (1995).
[5] J. J. Lee *et al.*, Circ. Res. **78**, 660 (1996).
[6] A. Karma, Phys. Rev. Lett. **65**, 2824 (1990); **71**, 1103 (1997); A. Winfree, Chaos **1**, 303 (1991); D. Barkley, Phys. Rev. Lett. **68**, 2090 (1992); M. Bar and M. Eiswirth, Phys. Rev. E **48**, R1635 (1993); H. Zhang and A. Holden, Chaos Solitons Fractals **5**, 661 (1995); D. Kessler *et al.*, Physica D **70**, 115 (1995); I. Efimov *et al.*, Chaos Solitons Fractals **5**, 513 (1995).
[7] A. Karma, Chaos **4**, 461 (1994); M. Courtemanche, *ibid.* **6**, 579 (1996).
[8] D. Zipes and J. Jalife, *Cardiac Electrophysiology: From Cell to Bedside*, 2nd ed. (W. B. Saunders Company, Philadelphia, 1995).
[9] T. Ikeda *et al.*, Circ. Res. **81**, 753 (1997).
[10] M. Graham *et al.*, Phys. Rev. E **52**, 76 (1995); N. Hartmann *et al.*, Phys. Rev. Lett. **76**, 1384 (1996).
[11] V. Zykov and S. Muller, Physica D **97**, 322 (1996); A. Pertsov *et al.*, *ibid.* **14**, 117 (1984).
[12] V. Zykov, *Simulations of Wave Processes in Excitable Media* (Manchester University Press, Manchester, 1988).
[13] H. Ito and L. Glass, Physica D **56**, 84 (1992); M. Courtemanche *et al.*, Phys. Rev. Lett. **70**, 2182 (1993); A. Karma *et al.*, Physica D **73**, 113 (1994); Z. Qu *et al.*, Phys. Rev. Lett. **78**, 1387 (1997).
[14] C. Luo and Y. Rudy, Circ. Res. **68**, 1501 (1991).
[15] Z. Qu and A. Garfinkel (unpublished).
[16] G. Strang, SIAM (Soc. Ind. Appl. Math.) J. Numer. Anal. **5**, 506 (1968).
[17] In the Luo-Rudy model action potential voltage ranges from -84 to 40 mV. We define action potential duration (A) as the period in which $V > -72$ mV, and while the period $V < -72$ mV, the diastolic interval (I). Action potential duration (A) restitution and wave conduction velocity (C) restitution are defined as their values versus the previous diastolic interval (I).
[18] Z. Qu and A. Garfinkel (unpublished).